Towards Integrated Microultrasound Systems

Bartas Abaravičius[1], Alexandru Moldovan[2], Srinjoy Mitra[1] and Sandy Cochran[2]
[1]Scottish Microelectronics Center, the University of Edinburgh, Edinburgh, UK
[2]James Watt School of Engineering, University of Glasgow, Glasgow, UK
babaravi@ed.ac.uk

***Abstract*—High-frequency ultrasound (HFUS) has been gaining traction to achieve high-resolution subsurface images of human tissue. Such capability could be used to locate lesions in the gastrointestinal tract (GIT), leading to early diagnosis of GIT disorders, which is directly correlated with a positive outcome of treatment. Hence, it is important to develop system components that aid HFUS development. Accordingly, this paper presents the setup, results and analysis of a pulse-echo test carried out with a custom, highly integrated, low-power pulser and a cross-coupled charge pump (CP). The system was tested with a 28 MHz linear ultrasonic (US) array using a bespoke low-power imaging protocol and the results were compared with a commercial research US system (Vantage™ 128, Verasonics®, WA, USA). The results verify the use of an integrated CP as a high-voltage source, as well as the capability of the pulser to generate 20 MHz signals – performance at 28 MHz could not be validated due to excessive ringing during tests. Strong parasitic effects were observed and their importance on efficient transmission is discussed.**

Keywords—Microultrasound, capsule endoscopy, pulser, pulse-echo, low-power.

I. Introduction

Video capsule endoscopy (VCE) is a medical procedure that allows visual inspection of the entire gastrointestinal tract (GIT) with reduced patient discomfort and a lower risk of complications compared to the traditional tethered endoscopy approach [1]. VCE technology was invented by Iddan *et al.* [2] and approved for human use by the FDA in 2001 [3]. It is particularly valuable for inspecting the small bowel epithelia as conventional endoscopes cannot reach that part of the GIT, and other visualization approaches, such as intraoperative enteroscopy, are complex and pose significant risks [4].

One of the main issues associated with VCE is that it can scan only the surface of the GIT, while subsurface inspection of lesions is often important in a clinical context for the correct diagnosis e.g. of Crohn's disease. Autofluorescence [5] and narrowband imaging [6] improve the mucosa's visibility and underlying vasculature of the scanned tissue, but the penetration depth is limited because of light absorbance. The incorporation of a microultrasound (μUS) transducer (operating frequency > 20 MHz) in a capsule endoscope (CE) would allow the device to scan deeper inside the tissue, while the high frequency of the probe allows for a more detailed image of the target [5]. Used in conjunction with the camera in a VCE device, the μUS system could potentially provide enhanced information of the scanned lesions due to the additional subsurface information and thus lead to better diagnosis.

Despite the potential advantages of the method, relatively little research has been published so far in μUS-enabled CE. Such devices either comprise a mechanically rotating single-element transducer [7], [8] or several single-element transducers [9]. These prototypes were successfully able to image the subsurface structures of GIT tissues in-vitro and in-vivo, but the devices were all tethered. Hence, the natural approach for the future development of an autonomous, ingestible CE is the miniaturization and incorporation of the driving and reception electronics into the capsule itself. This will, however, require significant electronic development.

In this paper, therefore, we report on the testing of integrated custom driving electronics comprising a high-voltage, single output pulser and a cross-coupled charge pump (CCCP) for high-voltage generation with a μUS 28 MHz transducer array with a fractional bandwidth of 60%. The tests were aimed to evaluate the driving capabilities of the electronics whilst comparing their performance with a commercial research ultrasound system (RUS) (Vantage™ 128, Verasonics®, WA, USA) employing the same driving parameters. A pulse-echo test with 3, 5 and 7-element Tx groups of the array elements was chosen as the means of comparison and the data obtained was analyzed in the time and frequency domains.

Instead of single-element transducers reported in prior CE prototypes, the array implementation will potentially lead to improved scan quality due to electronic steering and focusing of the US beam. It will also allow for further miniaturization of the capsule components due to the removal of the motor. However, an array-based design must meet restrictions of limited onboard power, high element count and parasitic effects. The work reported here represents a step towards the development of a wireless μUSCE system.

II. Materials and Methods

A. Integrated Pulser and High-voltage Generator

The integrated circuits (ICs) used in this work consisted of a high-voltage (HV) unipolar pulser to drive the μUS array and a CCCP to generate a regulated 20 V supply. Both circuits were developed on the same chip and were manufactured with the TSMC 130 nm Bipolar-CMOS-DMOS process.

The pulser was initially tested with 1.5 MHz and 3.0 MHz arrays and was presented previously [10]. It used a bootstrapped double-nMOS architecture which eliminated the current draw from the HV supply while its footprint was reduced compared to a complementary CMOS switch required for the same output current sourcing capability. The output stage was designed and verified with measurements to allow square wave generation with < 3 ns rise/fall times for output capacitive loads of < 550 pF whilst compensating for parasitic inductances between the IC and a transducer. The average power consumption of the pulser was 484 μW at a 100 kHz pulse repetition frequency (PRF) and peak currents of 13 A, allowing for low-power operation with a wide range of US transducers.

The integrated HV generator was based on a CCCP powered by a 3.1 V supply representing voltage achievable from two serially-connected silver-oxide coin cell batteries of the type conventionally used in CE devices [11]. The CCCP comprised 5 stages: the first stage was used to double the input to 6.2 V, followed by another four stages resulting in a total

ideal voltage gain of 10 and output voltage V_{OUT} = 31 V. Measurements of the circuit showed a maximum output voltage of 28 V at 10 µA load and exhibited peak efficiency of 58% at 350 µA load. The CCCP included a mode for a regulated output and could generate 20 V up to an average current of 500 µA.

B. Low Power Imaging Protocol

In order to be compatible with the limited power supply available inside the capsule, both average and instantaneous power consumption had to be decreased by reducing the number of transmitting (Tx) array elements from the entire aperture (128 elements) to a group of 3, 5 or 7 elements per acquisition event. The receiving (Rx) aperture was set to one element per acquisition to minimize the number of ADCs to be used in the CE. The data obtained per acquisition event was, therefore, an A-scan produced by the active Rx element of the array. A full frame (B scan) was then obtained by sweeping the 5 Tx/ 1Rx active elements across the array's entire aperture and merging the recorded A-scans (Figure 1). A detailed description and evaluation of this approach will be reported in a future publication.

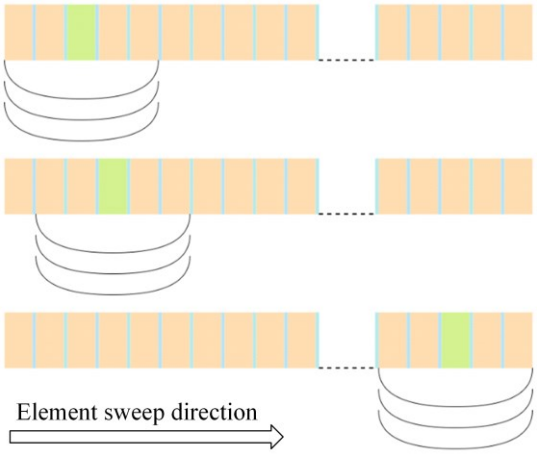

Figure 1. Custom imaging protocol using a group of 5 Tx elements and 1 Rx element for reduced power consumption.

C. Experimental Setup

The integrated pulser was tested in a pulse-echo setup, as shown in Figure 2. The pulse was generated by the integrated pulser or the RUS, both set to generate unipolar 20 V square pulses. The pulser was driven by an Agilent 33250A, which produced a 17 ns input pulse with a 5 ns edge time, while the RUS pulse was set by the centre frequency setting f_C = 28 MHz. The 20 V supply to the pulser was generated by a precision source measurement unit (SMU) (B2901B, Keysight, CA, USA). For comparison purposes, a single RUS channel was used for TX. In both cases, an average of 32 pulse-echo measurements were employed; this is consistent with the relatively slow motion of a CE through the GIT and the very short acquisition time needed for its shallow tissue depth (< 5mm) [12].

A 28 MHz array was placed at 6 mm in front of a quartz reflector mounted on an acoustic absorber and submerged in degassed water. The array used in this experiment (128 element, 28 MHz, Vermon, Tours, France) was housed on a flex-rigid PCB with two board-to-board connectors on each side. Two custom connector PCBs were used as the interface between the array and mini-coaxial cables. The signal path between the pulse source and the array elements encompassed

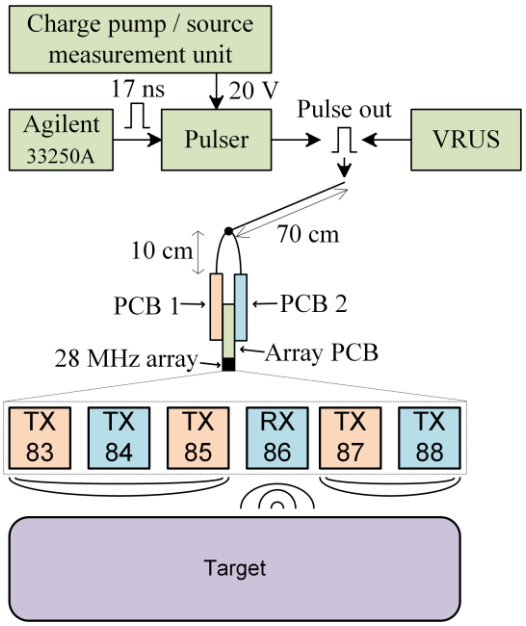

Figure 2. Diagram of the experimental setup with 5 TX elements. The colors of the elements indicate the PCB connecting them.

a 70 cm coaxial cable split in two 10 cm cables connecting to the PCBs, followed by a minimum-length, multi-thread copper wire shorting the elements on the PCBs.

A digital oscilloscope (DSOX2014A, Keysight, CA, USA) was used to record the TX waveform at the connector PCBs and the first echo signal at the RX element. The experiment was repeated with 3, 5 and 7 Tx elements shorted together. As the integrated pulser did not incorporate an on-chip TX/RX switch, an additional RX element was included in the centre-most location between the TX elements. While this arrangement resulted in asymmetrical TX patterns (e.g., 5-element setup: 3x TX + 1 RX + 2x TX), it did not hinder the relative comparison between the pulser and the RUS, although it had the potential to degrade performance compared with a symmetrical setup.

III. Results

The results of a (5 TX + 1 RX) setup are discussed, followed by a breakdown of critical parameters between different element tests. The time plot of the 5 TX pulse measured at the connector PCBs is shown in Figure 3(a). The signal from the RUS reached 17.6 V and the pulser peaked at 27 V with a benchtop supply and at 25 V using the integrated CCCP. While the initial pulse from 0 V to 20 V in both RUS and pulser setups was triangular in nature, the RUS pulse was significantly more damped, producing a single 21 V pulse with an undershoot on the falling edge of -7.3 V and settling time of 143 ns. In contrast, the first peak from the pulser was 27.3 V, and a strong reverberation was observed, settling at 10% of the 20 V value within 330 ns. The CCCP-powered pulser setup resulted in the same output, but with an overall lower amplitude. The frequency spectrum of the TX pulse is shown in Figure 3 (b). The plot shows a wide bandwidth signal generated by the RUS with a peak at 8.6 MHz, significantly below f_C = 28 MHz. The pulser setup behaviour was narrowband, centred at 20.7 – 20.8 MHz.

The echo signal measured in a 5 TX setup is shown in Figure 4 (a). The signal reaches over 50 mV peak-to-peak with the SMU supply and 40 mV with the CCCP compared to 14 mV in the RUS setup. The ringing observed in the pulser TX is also present in the echo waveform. The frequency

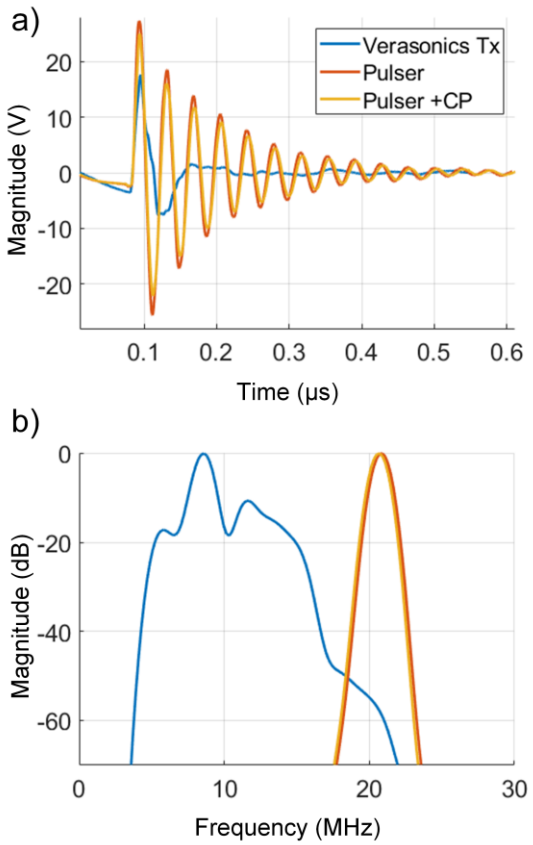

Figure 3. Measurement results of a 5 TX setup: a) waveform measured at PCBs 1 and 3; b) relative power distribution in frequency of the TX.

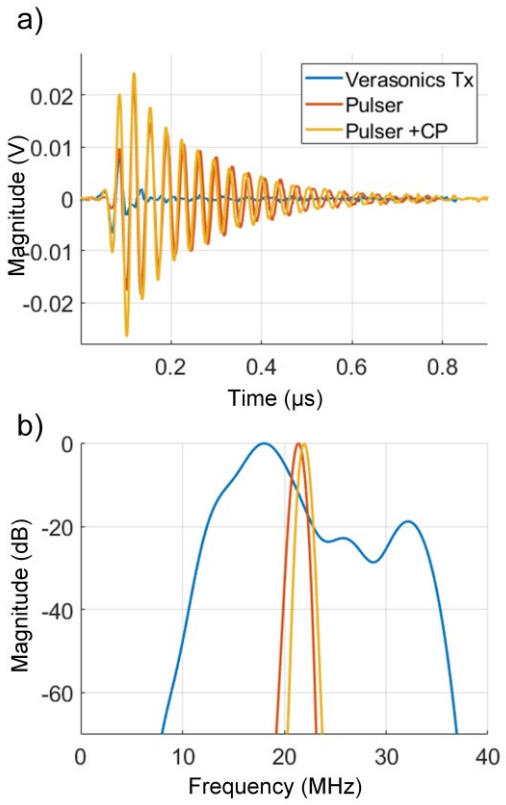

Figure 4. Echo measured with a 5 TX setup: a) waveform b) relative power distribution in frequency of the Rx signal.

response in Figure 4 (b) identifies a broader bandwidth of the echo resulting from the RUS pulse, spanning 9 - 36 MHz (-60 dB range) and with peak power at 18 MHz and a second local peak at 32.2 MHz. A local minimum is present at around 28 MHz. In contrast, the echo from the two pulser setups is equivalent to the TX distribution: most of the signal power is in the range 19 – 24 MHz (-60 dB range), with the centre at 21.45 MHz and 22 MHz for the SMU and CCCP powered setups respectively.

The experiment was repeated for 3 and 7-element setups and resulted in waveforms with the same characteristics: a narrow band with a centre around 21.5 – 22 MHz in pulses generated with the integrated pulser and wideband signals in the RUS setups. The results from all 3, 5 and 7 element tests are summarised in Table 1. The results with an SMU-powered pulser led to higher peak-to-peak values but did not change other waveform parameters compared to CP-powered setups; thus only results of the latter are given in conjunction with the VRUS measurements.

Table 1. Summary of the measurements with 3, 5 and 7 Tx elements.

Number of elements			3	5	7
First peak amplitude (V)	Tx	Pulser	34	27	27
		VRUS	23.7	21	17.5
Peak-to peak (mV)	Rx	Pulser	36	50	44.29
		VRUS	16.7	14	34.1
Frequency of maximum power (MHz)	Tx	Pulser	26.2	20.9	20.5
		VRUS	11.5	8.6	8.6
	Rx	Pulser	27.6	21.3	21.5
		VRUS	17.6	18	18.3
Signal duration (ns)	Tx	Pulser	249	330	346
		VRUS	126	143	176

IV. Discussion

Based on the results, the RUS transmission pulse was lower in magnitude, strongly damped and centred around lower frequencies compared to the integrated pulser setup. It also exhibited power distribution over a broader frequency range. In the integrated pulser setup, most of the power was centred around the frequency at which the circuit was ringing, and so, with other frequency components present at much lower levels, below – 60 dB, it signifies low power efficiency concerning the desired 28 MHz. This fact is reinforced by the frequency response of the echo signal, which encompassed higher frequency components in RUS tests but was almost identical to the TX waveform in the integrated pulser tests.

The oscillation observed in the integrated pulser signals was linked to high parasitic effects. The connector PCBs and mini-coaxial interconnects were a constant between the RUS and integrate pulser setups but, in the latter case, additional parasitic components were present due to wire-bonding and the PCB housing the IC. The effects of these components were exacerbated by the high current sourcing capability of the pulser, leading to higher TX/RX amplitudes and oscillation of the parasitic circuit at the input of the array, hindering efficient driving. Preliminary tests with higher capacitance, lower inductance and resistance parasitic components - observed during the development of the test setup and not shown here - resulted in improved ringing but lower echo amplitudes, signifying strong dependence of the performance of the pulser on its interface with the array.

V. Conclusions and Future Work

This work aimed to investigate the capabilities of an integrated pulser, powered by an on-chip cross-coupled charge pump, and to compare the response with a commercial RUS. The measurements indicated narrowband behaviour of the custom electronic setup which was highly influenced by the parasitic effects. Nonetheless, the echo signals in the pulser setup were higher in magnitude, and further tests, including the CCCP, showed only a fractional drop in the amplitude across signals compared to an ideal source. This validates low power and highly integrated high-voltage generation on-chip capability for µUS pulse generation.

The final goal of a µUS capsule endoscope entails very close integration between the integrated electronics and the ultrasound array. For these reasons, a new, more compact test setup is needed to minimize parasitic influences and improve comparison quality. This will be reported in due course. Furthermore, the results provided here used a single output pulser as the driving device, and a multi-output pulser with better optimization is under development for future prototypes.

Acknowledgements

This work was carried out as part of the AUTOCAPSULE project aimed at developing an autonomous multimodal implantable endoscopic capsule for the gastrointestinal tract. The project has received funding from European Union's Horizon 2020 Research and Innovation Programme under Grant Agreement No. 925118.

The integrated electronics used in the tests were designed and manufactured using funding from Dialog Semiconductor, A Renesas Company.

References

[1] M. E. Riccioni, R. Urgesi, R. Cianci, A. Bizzotto, C. Spada, and G. Costamagna, "Colon capsule endoscopy: Advantages, limitations and expectations. Which novelties?," *World J Gastrointest Endosc*, vol. 4, no. 4, pp. 99–107, Apr. 2012, doi: 10.4253/wjge.v4.i4.99.

[2] G. Iddan, G. Meron, A. Glukhovsky, and P. Swain, "Wireless capsule endoscopy," *Nature*, vol. 405, no. 6785, Art. no. 6785, May 2000, doi: 10.1038/35013140.

[3] C. Van de Bruaene, D. De Looze, and P. Hindryckx, "Small bowel capsule endoscopy: Where are we after almost 15 years of use?," *World J Gastrointest Endosc*, vol. 7, no. 1, pp. 13–36, Jan. 2015, doi: 10.4253/wjge.v7.i1.13.

[4] M. Pennazio, E. Rondonotti, and R. de Franchis, "Capsule endoscopy in neoplastic diseases," *World J Gastroenterol*, vol. 14, no. 34, pp. 5245–5253, Sep. 2008, doi: 10.3748/wjg.14.5245.

[5] G. Cummins *et al.*, "Gastrointestinal diagnosis using non-white light imaging capsule endoscopy," *Nat Rev Gastroenterol Hepatol*, vol. 16, no. 7, Art. no. 7, Jul. 2019, doi: 10.1038/s41575-019-0140-z.

[6] R. Singh, V. Owen, A. Shonde, P. Kaye, C. Hawkey, and K. Ragunath, "White light endoscopy, narrow band imaging and chromoendoscopy with magnification in diagnosing colorectal neoplasia," *World J Gastrointest Endosc*, vol. 1, no. 1, pp. 45–50, Oct. 2009, doi: 10.4253/wjge.v1.i1.45.

[7] J. H. Lee, G. Traverso, D. Ibarra-Zarate, D. S. Boning, and B. W. Anthony, "Ex Vivo and In Vivo Imaging Study of Ultrasound Capsule Endoscopy," *J Med Device*, vol. 14, no. 2, p. 021005, Jun. 2020, doi: 10.1115/1.4046352.

[8] Y. Qiu *et al.*, "Ultrasound Capsule Endoscopy With a Mechanically Scanning Micro-ultrasound: A Porcine Study," *Ultrasound Med Biol*, vol. 46, no. 3, pp. 796–804, Mar. 2020, doi: 10.1016/j.ultrasmedbio.2019.12.003.

[9] H. S. Lay *et al.*, "In-Vivo Evaluation of Microultrasound and Thermometric Capsule Endoscopes," *IEEE Trans Biomed Eng*, vol. 66, no. 3, pp. 632–639, Mar. 2019, doi: 10.1109/TBME.2018.2852715.

[10] B. Abaravicius, A. Moldovan, S. Cochran, and S. Mitra, "Development of a Point-of-Care Ultrasound Driver for Applications with Low Power and Reduced Area Requirements," in *2021 IEEE International Ultrasonics Symposium (IUS)*, Xi'an, China, Sep. 2021, pp. 1–4. doi: 10.1109/IUS52206.2021.9593342.

[11] C. Steiger, A. Abramson, P. Nadeau, A. P. Chandrakasan, R. Langer, and G. Traverso, "Ingestible electronics for diagnostics and therapy," *Nat Rev Mater*, vol. 4, no. 2, pp. 83–98, Feb. 2019, doi: 10.1038/s41578-018-0070-3.

[12] H. S. Lay, B. F. Cox, V. Seetohul, C. E. M. Demore, and S. Cochran, "Design and simulation of a ring-shaped linear array for microultrasound capsule endoscopy," *IEEE Transactions on Ultrasonics, Ferroelectrics, and Frequency Control*, vol. 65, no. 4, pp. 589–599, 2018, doi: 10.1109/TUFFC.2018.2794220.